Journal of Oceanography, Vol. 59, pp. 461 to 475, 2003

Interdecadal Variation of the Transition Zone Chlorophyll Front: A Physical-Biological Model Simulation between 1960 and 1990

Fei Chai[1]*, Mingshun Jiang[1], Richard T. Barber[2], Richard C. Dugdale[3] and Yi Chao[4]

[1]*School of Marine Science, 5471 Libby Hall, University of Maine, Orono, ME 04469-5741, U.S.A.*
[2]*Duke University, NSOE Marine Laboratory, 135 Duke Marine Lab Road, Beaufort, NC 28516, U.S.A.*
[3]*Romberg Tiburon Center, San Francisco State University, PO Box 855, Tiburon, CA 94920, U.S.A.*
[4]*Jet Propulsion Laboratory, California Institute of Technology, 4800 Oak Grove Drive, Pasadena, CA 91109, U.S.A.*

(Received 25 June 2002; in revised form 30 November 2002; accepted 5 December 2002)

The interdecadal climate variability affects marine ecosystems in both the subtropical and subarctic gyres, consequently the position of the Transition Zone Chlorophyll Front (TZCF). A three-dimensional physical-biological model has been used to study interdecadal variation of the TZCF using a retrospective analysis of a 30-year (1960–1990) model simulation. The physical-biological model is forced with the monthly mean heat flux and surface wind stress from the COADS. The modeled winter mixed layer depth (MLD) shows the largest increase between 30°N and 40°N in the central North Pacific, with a value of 40–60% higher during 1979–90 relative to 1964–75 values. The winter Ekman pumping velocity difference between 1979–90 and 1964–75 shows the largest increase located between 30°N and 45°N in the central and eastern North Pacific. The modeled winter surface nitrate difference between 1979–90 and 1964–75 shows increase in the latitudinal band between 30°N and 45°N from the west to the east (135°E–135°W), the modeled nitrate concentration is about 10 to 50% higher during the period of 1979–90 relative to 1964–75 values depending upon locations. The increase in the winter surface nitrate concentration during 1979–90 is caused by a combination of the winter MLD increase and the winter Ekman pumping enhancement. The modeled nitrate concentration increase after 1976–77 enhances primary productivity in the central North Pacific. Enhanced primary productivity after the 1976–77 climatic shift contributes higher phytoplankton biomass and therefore elevates chlorophyll level in the central North Pacific. Increase in the modeled chlorophyll expand the chlorophyll transitional zone and push the TZCF equatorward.

Keywords:
· Pacific decadal variability,
· physical-biological modeling,
· chlorophyll front,
· Pacific Ocean,
· model simulation.

1. Introduction

The North Pacific Transition Zone (NPTZ) is bounded by two oceanographic fronts at approximately 30–32°N (Subtropical Front) and 42–45°N (Subarctic Front) in the central Pacific (Roden, 1991). The northern boundary of the subtropical gyre, the Subtropical Front, is defined as the surface outcropping of the 17°C isotherm and 34.8 isohaline (Roden, 1991), and it can migrate a few degrees latitudinally on seasonal and interannual time scales (Lynn, 1986). The best marker of the Subarctic Front is the 33 isohaline in the salinity front with lower salinity water located in the subarctic region (Favorite *et al*., 1976). Using the data collected on board the commercial cargo carrier *M/V Skaugran* between January 1995 and January 2001, Wong *et al*. (2002) documented the seasonal and interannual changes in surface properties in the north of the Subarctic Front and discussed in detail the differences and similarities between the eastern and western subarctic regions.

The Transition Zone Chlorophyll Front (TZCF) is a biological front within the NPTZ that separates the low chlorophyll subtropical gyres and the high chlorophyll subarctic gyres in the Pacific Ocean. Operationally, the TZCF is defined as the location of 0.2 mg/m^3 surface

* Corresponding author. E-mail: fchai@maine.edu

chlorophyll (Polovina *et al*., 2001). The TZCF migrates seasonally due to the extension or contraction of subtropical and subarctic gyres. Analyzing satellite maps of surface chlorophyll in the North Pacific, Polovina *et al*. (2001) documented the TZCF which is over 8000 km in longitude with a winter position around 30°N and summer position around 40°N. The position and dynamics of the TZCF varied substantially during the 1998 El Niño and the 1999 La Niña (Polovina *et al*., 2001).

With just a few years of high resolution basin-wide SeaWiFS surface chlorophyll coverage, it is apparent that the TZCF is a dynamic feature that strongly influences pelagic marine resources. The location of the TZCF appears to be related to juvenile albacore tuna migration patterns within the transition zone (Polovina *et al*., 2001) and it has potential implications for albacore fishery. The TZCF has also been revealed as an important foraging and migration pathway for loggerhead turtles (*Caretta caretta*) in the central North Pacific by tracking turtles using satellite telemetry and comparing their routes with the TZCF observed by satellite (Polovina *et al*., 2000).

The high quality remote sensing ocean color data, i.e., SeaWiFS and OCTS, have been available only for the past several years (1997 to present). There is a big gap between the CZCS data set (1978–86) and the SeaWiFS, so detecting the interdecadal migration of the TZCF using the remote sensing data is not possible at present. Sparse observations suggest that the position of the front varies on the interdecadal time scale but the limited chlorophyll measurements cannot provide a complete description of how the TZCF migrates in response to the Pacific Decadal Oscillation (PDO). Since the interdecadal climate variability significantly affects marine ecosystems in both subtropical and subarctic gyres (McGowan *et al*., 1998; Karl *et al*., 2001), it must consequently affect the positions of the TZCF.

Based upon the Hawaii Ocean Time-series (HOT) program and the limited historical data, Karl *et al*. (2001) reported that primary productivity in the subtropical gyre increased after the 1976–77 regime shift. Analyzing and comparing apparent oxygen utilization (AOU) from four meridional transects through the northeast subtropical Pacific between 1980 and 1997, Emerson *et al*. (2001) found an increase in AOU by 20–25% over the past two decades and suggested that an increase in oxygen demand by the biological pump and/or oxygen degassing by upper-ocean ventilation were accountable for the observed AOU increase.

Interdecadal physical variability in the subarctic Pacific has been observed in a number of ocean and atmospheric variables (Trenberth and Hurrell, 1994). One of the well-documented climatic changes in the North Pacific occurred during the period 1976–77, when the intensification of the Aleutian Low pressure system resulted in a southward shift of the westerly winds, a stronger winter circulation at mid-latitudes, and enhanced surface ocean sensible and latent heat fluxes (Graham, 1994; Miller *et al*., 1994). Variations of oceanic physical variables have a series of implications on marine ecosystems (Mantua *et al*., 1997; Sugimoto and Tadokoro, 1997; McGowan *et al*., 1998). Widespread ecological changes associated with the 1976–77 climatic shift were observed throughout the North Pacific Ocean, ranging from plankton to the higher trophic levels (Venrick *et al*., 1987; Polovina *et al*., 1994; Francis and Hare, 1994). In the northwestern subtropical gyre region, chlorophyll in the spring showed a steady increase from the mid 1970s to the mid 1980s (Limsakul *et al*., 2001).

The dynamic linkages between ocean physics and biology on an interdecadal scale are poorly understood because it is difficult to sample at the time and space scales necessary to elucidate the connections between large-scale physical processes and the smaller-scale biological responses (Miller and Schneider, 2000). In contrast, physical-biogeochemical models that express the interrelationships mathematically between physical forcing and the responses of ecosystem and biogeochemical processes can provide the necessary time and space scale resolution. Several basin scale ecosystem model studies, explicitly including the upper ocean biological processes, have been carried out recently. Chai *et al*. (1996, 1999) incorporated an ecosystem model into a primitive equation circulation model to study nutrient cycles in the high nutrient and low chlorophyll (HNLC) environment for the equatorial Pacific. Kawamiya *et al*. (2000a, b) embedded a six-component ecosystem into an ocean general circulation model (OGCM) of the North Pacific, and successfully reproduced spatial distribution and seasonal variations of biological variables. Haigh *et al*. (2001) embedded a simple biological model in an isopycnic general circulation model, and their physical-biological model reasonably reproduced the spatial patterns and seasonal changes in SeaWiFS images. Moreover, their modeled results showed a deepening of the mixed layer depth in the subtropical gyres and shallowing in several regions of the subpolar gyres, which increased the modeled nutrient concentration in the subtropical regions after 1976, correlated with increased plankton biomass.

Analyzing the estimated winter and spring mixed layer depth (MLD) from the National Oceanographic Data Center (NODC) temperature data, Polovina *et al*. (1995) found that winter and spring MLD in the subtropical and transition zone was 30–80% greater during 1977–88 than during 1960–76, while in the subarctic zone the MLD was 20–30% shallower. They also employed a simple plankton model forced with observed MLD and nutrients, and found that deepening in the mixed layer might increase phytoplankton production in nutrient-poor subtropical

regions by supplying more nutrients from depth, shallowing MLD in the subarctic would also increase production by increasing the availability of light to phytoplankton cells within the mixed layer. In between the subtropical and subarctic regions, both nutrient supply and light availability likely co-limit phytoplankton production, but how these processes change on the interdecadal time scale is not clear.

In order to improve our understanding of the dynamics that control the position of the TZCF and its interdecadal variability, we present a 30-year (1960–1990) retrospective analysis of the Pacific Ocean based upon the physical-biological model simulation. Our goal is to provide modeled evidence of interdecadal changes in the TZCF position and identify the responsible factors.

2. Model Description

2.1 Physical circulation model

The physical model is the oceanic component of the National Center for Atmospheric Research (NCAR) Climate System Model (CSM) (Gent *et al*., 1998), which is a modified version of the Geophysical Fluid Dynamic Laboratory (GFDL) Modular Ocean Model (MOM 1.0, Pacanowski *et al*., 1991). We have configured the model for the Pacific Ocean and the model performance has been reported in Li *et al*. (2001). The nonlocal KPP mixing scheme developed by Large *et al*. (1994) is incorporated into the model to better capture the small-scale physics within upper mixed layer and interior internal waves and double diffusion activities in the deep ocean. The Gent and McWilliam (1990) eddy-induced isopycnal mixing parameterization is applied. A third order upwind differencing scheme (Holland *et al*., 1998) is used to compute all tracers including temperature, salinity and biochemical components. The horizontal and vertical background mixing coefficients tracers (temperature, salinity, and all biological components) are chosen to be 2×10^6 cm^2/sec and 0.1 cm^2/sec, respectively. The latter turns out to be critical to maintain realistic vertical patterns of tracers within the thermocline. The vertical viscosity (for velocity calculation) is chosen to be 1.0 cm^2/sec, an order larger than background mixing, while the horizontal viscosity is 5×10^6 cm^2/sec.

The Pacific Ocean model domain is between 45°S and 65°N, 100°E and 70°W, with realistic geometry and topography. The longitudinal resolution of the equatorial Pacific is 2° everywhere, while the latitudinal is 0.5° within 10°S and 10°N, tapering off to 2° at high latitude. There are 40 vertical layers, with 23 levels located in the upper 400 m. The boundaries at 45°S and 65°N are closed walls and no flow is allowed through the boundary. In the regions near the two closed walls, a sponge layer of 10° wide from the walls is applied. A decay term κ(T*–T) is added to the tracer equations with T representing temperature, salinity, nitrate and silicate. T* represents the observed temperature, salinity, nitrate and silicate fields taken from NODC World Ocean Atlas (Levitus *et al*., 1994). The κ values vary smoothly from 50 day^{-1} at the north or south walls to zero at 10° away from the walls.

2.2 Biological model

The biological model was developed originally to study the nitrogen and silicon cycles in the equatorial Pacific (Chai *et al*., 2002; Dugdale *et al*., 2002; Jiang *et al*., 2003). The 1-D model has been tested against the JGOFS data over the equatorial Pacific and is capable of reproducing the Low-Silicate, High-Nitrate, Low-Chlorophyll (LSHNLC) conditions in the equatorial Pacific. The biological model (Fig. 1) consists of ten compartments describing two size classes of phytoplankton (P1, P2) and zooplankton (Z1, Z2), detrital nitrogen (DN) and detrital silicon (DSi), silicate ($Si(OH)_4$), and total CO_2 and two forms of dissolved inorganic nitrogen: nitrate (NO_3) and ammonium (NH_4), which are treated separately, thus enabling division of primary production into new and regenerated production. P1 represents small, easily grazed phytoplankton whose specific growth varies, but whose biomass is regulated by micrograzers (Z1) and whose daily net productivity is largely remineralized (Landry *et al*., 1997). P2 represents relatively large phytoplankton (>5 μm) that makes up high biomass blooms and contributes disproportionately to sinking flux as ungrazed production or large fecal pellets (Wefer, 1989; Bidigare and Ondrusek, 1996). The P2 class represents the diatom functional group, and has the potential to grow rapidly under optimum nutrient conditions (Coale *et al*., 1996). Z1 represents small micrograzers whose specific growth rate is similar to P1 phytoplanktons whose grazing rate is density dependent (Landry *et al*., 1997), and Z2 represents the larger mesozooplankton that graze on P2 and detrital nitrogen (DN) and prey on Z1. The Z2 zooplankton have a feeding threshold with conventional grazing dynamics as described in Frost and Franzen (1992).

Below the euphotic zone, sinking particulate organic matter is converted to inorganic nutrients by a regeneration process similar to the one used by Chai *et al*. (1996), in which organic matter decays to ammonium and is then nitrified to NO_3. The flux of particulate material is specified using an empirical function taken from Martin *et al*. (1987). The silicate regeneration is modeled through a similar approach but with a deeper regeneration depth profile, which reflects the fact that biogenic silica tends to have a higher preservation efficiency than other particulate organic matter (Ragueneau *et al*., 2000). The detailed equations and parameters used for the biological model were presented in the paper by Chai *et al*. (2002).

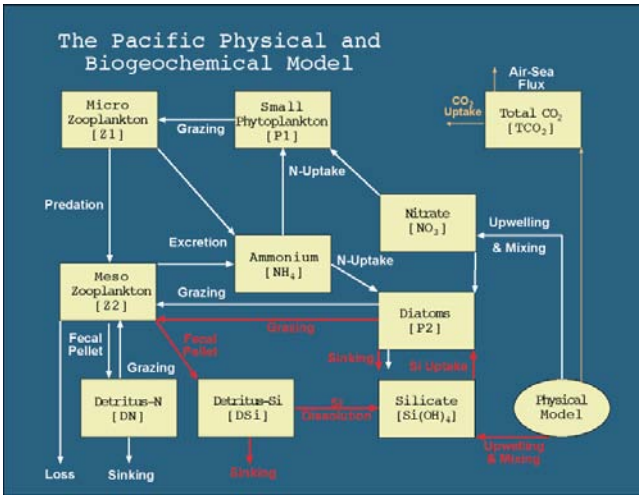

Fig. 1. The inter-compartmental flow chart of the ecosystem and linkage to carbon and physical processes in the euphotic zone. The flow of nitrogen is indicated by solid line; the flow of silicon is indicated by a dashed line and the carbon flow is indicated by a line-dashed line.

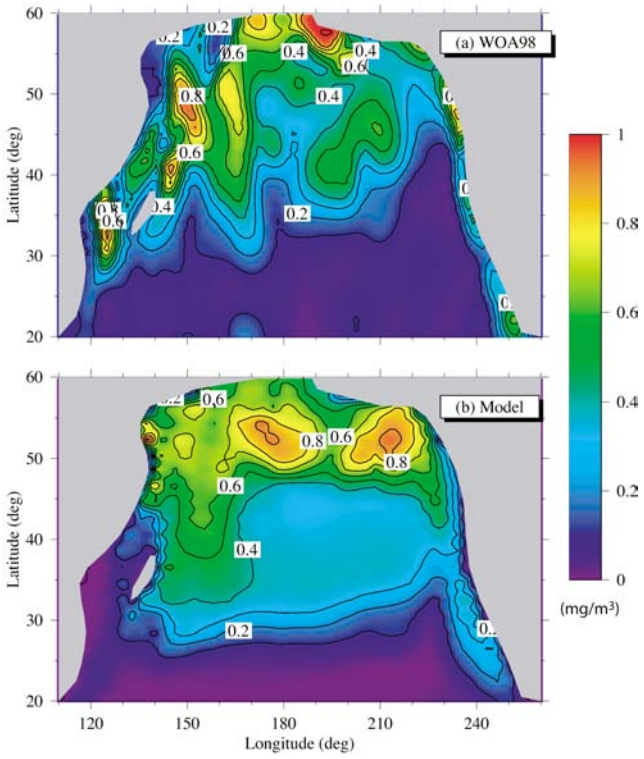

Fig. 2. Comparisons of the modeled surface chlorophyll and WOA98 data in spring (April–May–June) (unit: mg/m^3). The modeled surface chlorophyll concentration was derived from the modeled top layer (5 m) phytoplankton biomass concentration (mmol N/m^3), that was converted to mg/m^3 using a nominal gram chlorophyll to mole nitrogen ratio of 1.58, which corresponds to a chlorophyll to carbon mass ratio of 1:50 and a C:N mole ratio of 6.625.

2.3 Initial conditions and surface forcing

The physical model is initialized with NODC World Ocean Atlas climatological January temperature and salinity (Levitus and Boyer, 1994; Levitus *et al*., 1994) with zero velocities. The nutrients (nitrate and silicate) are initialized with NODC World Ocean Atlas climatological annual mean values (Levitus *et al*., 1993). For other components in the biological model, they are assigned with 0.25 mmol m^{-3} at the surface, decreasing exponentially with a scale length of 120 m, which is the depth of the euphotic zone. Chai (1995) showed that the initial conditions in the euphotic zone for the biological model did not alter the final results because the biological model reached the equilibrium faster than the physics did.

The surface forcing can be separated into momentum, heat, fresh-water fluxes, and light for the photosynthesis. The momentum fluxes are calculated with the zonal and meridional wind speeds from the Comprehensive Ocean Atmosphere Data Set (COADS) (da Silva *et al*., 1994). COADS is selected because it is the longest surface marine dataset covering the entire Pacific Ocean. The heat flux calculation includes short wave radiation, outgoing long wave radiation, and both sensible heat and latent heat fluxes. The surface salinity is restored to the NODC climatological monthly mean salinity (Levitus *et al*., 1994). More details about surface physical forcing treatment can be found in Li *et al*. (2001). The surface light intensity (I_o) is converted from the monthly mean COADS short wave radiation (R_s) using $I_o = 0.5*R_s$. Since the monthly averaged short wave radiation is used, the day-night cycle of light is not resolved in the current model, rather the daily averaged light is used for photosynthesis calculation.

The equations governing the ecosystem are solved simultaneously with the physical model. The physical-biological model is integrated for 10 years from the initial conditions. During this 10-year period, the model achieves a quasi-equilibrium state of annual cycle in the upper ocean. Monthly mean forcing from January 1955 to December 1993 is then used to force the coupled physical-biological model. This paper focuses on the model results for the period between January 1960 and December 1990.

3. Results and Discussion

3.1 Modeled seasonal migration of the TZCF

Based upon the same circulation model configurations, the model performance of the physical conditions and its variability have been reported by Li *et al*. (2001).

By comparing two different vertical-mixing schemes, Pacanowski and Philander (PP) and K-Profile Parameterization (KPP), Li *et al*. (2001) found that KPP is significantly better than the PP scheme in simulating the thermal and current structures, including the annual mean, annual cycle, and interannual-to-interdecadal variability. Li *et al*. (2001) also documented comparisons in detail between the modeled physical properties with the observations. In this paper we focus on the modeled ecosystem response to physical variability in the central North Pacific.

The Pacific Ocean is by far the largest ocean in the world. Its immense size is reflected in great spatial differences in mixed layer depth, thermocline depth, upwelling velocity, and other physical features, which results in diverse regional oceanic ecosystems (Longhurst, 1998). The biological processes respond to variations in physical forcing functions such as solar radiation and surface wind on a variety of timescales, spring bloom of phytoplankton biomass is the dominant temporal feature in the western subarctic gyres, and it is essential for biological models to capture spring blooms both in terms of spatial pattern and intensity (Frost and Kishi, 1999). The modeled spring (April–May–June) surface chlorophyll, converted from the modeled phytoplankton biomass, compares well with the historical *in situ* chlorophyll measurements in the western and central subarctic regions (NODC World Ocean Atlas 1998, Conkright *et al*., 1998), Fig. 2.

On the other hand, in the northeast subarctic region the model tends to produce surface chlorophyll levels that are higher than the observational data. At the Ocean Station Papa (OSP) at 50°N and 145°W in the subarctic Northeast Pacific, surface chlorophyll only increases slightly during late spring and early summer, from 0.2 to 0.4 mg/m^3 (Harrison, 2002), whereas the modeled spring and early summer surface chlorophyll level is around 0.6 to 0.8 mg/m^3, about a factor of 2 higher than the observations. This is mainly due to inadequate treatments of iron limitation for the subarctic Northeast Pacific with the present ecosystem model structure. The OSP has been characterized as a high nitrate and low chlorophyll (HNLC) region where iron limits the growth of large diatoms in late spring and summer (Martin and Fitzwater, 1988), iron and irradiance co-limit in the winter (Maldonado *et al*., 1999). The current ecosystem model takes account of the role of iron for the equatorial Pacific Ocean, also a HNLC region, by incorporating the effects of iron limitation implicitly through the parameters that determine the growth rate of diatoms (Chai *et al*., 2002). Several iron enrichment experiments were conducted by changing the parameter α (the initial slope of the photosynthetic rate over irradiance at low irradiance) and $\mu 2_{max}$ (the potential maximum specific diatom growth rate) in the regulation terms of silicate uptake by diatom (Chai *et al*., 2002). The values for these parameters were selected based upon observations made for the equatorial Pacific Ocean (Barber and Chavez, 1991; Barber *et al*., 1996), which may not be suitable for the OSP in the subarctic Northeast Pacific. Denman and Pena (1999) developed an ecosystem model for the OSP and addressed the iron limitation implicitly with a similar approach to that used by Chai *et al*. (1996, 1999) for the equatorial Pacific. Due to the drastic differences between the model structures, it is unlikely at present that we can incorporate iron limitation properly for both the equatorial Pacific and the subarctic Northeast Pacific at the same time. In summary, our present ecosystem model has a weaker iron limitation for the OSP and it therefore produces stronger spring to summer chlorophyll transition, and the phytoplankton seasonal cycle is determined mainly by the light limitation and the depth of the mixed layer. In the future, ecosystem model development needs to consider the iron limitation explicitly which can produce multiple HNLC regions simultaneously.

Due to a lack of horizontal resolution (2° in longitude) near the coastal regions, the model does not resolve chlorophyll conditions associated with the coastal upwelling, such as along the coast of California. The domain of this physical-biological model was designed to study oceanic biological processes on the basin-scale and it is therefore not suitable for investigating coastal processes.

In the subtropical gyre (south of 28°N), both the modeled and *in situ* chlorophyll concentrations tend to be much lower than in the subarctic region, around 0.1 mg/m^3 or less. A biological front, normally located between 28°N and 40°N, that separates the low chlorophyll subtropical gyres and the high chlorophyll subarctic gyres in the Pacific Ocean, is refered to as the Transition Zone Chlorophyll Front (TZCF) (Polovina *et al*., 2001). Analyzing remote sensing images of surface chlorophyll, Polovina *et al*. (2001) found that a chlorophyll concentration of 0.2 mg/m^3 is a good indicator of the TZCF positions. The isopleth of 0.2 mg/m^3 chlorophyll migrates seasonally due to the extension or contraction of subtropical and subarctic gyres. For example, during the winter season (January to March), a 0.2 mg/m^3 chlorophyll front is located between 26°N and 27°N in the central Pacific, and it is located between 34°N and 35°N during the summer season, as shown in Fig. 3. During the winter and early spring, stronger vertical mixing enhances the supply of nutrients and photosynthetic available radiation (PAR) is relatively adequate in the TZCF, especially in the southern section. These conditions are favorable for enhancing phytoplankton growth, which results in pushing the 0.2 mg/m^3 chlorophyll front equatorward to between 26°N and 27°N. On the other hand, an increase in

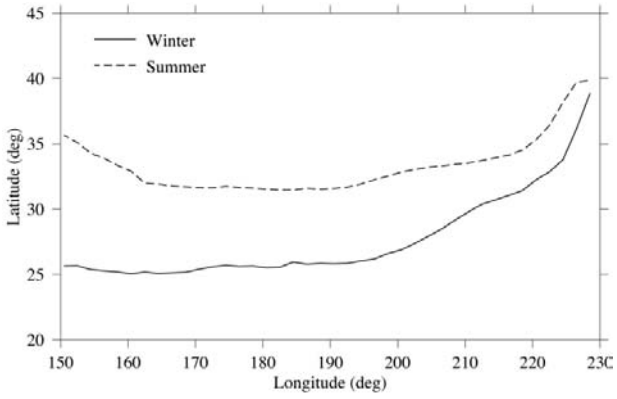

Fig. 3. The locations of the transition zone chlorophyll front (chlorophyll = 0.2 mg/m^3) during the climatological winter (January–February–March) and summer (July–August–September).

surface heat flux into the ocean results in stronger stratification during the summer (July to September), which reduces vertical nutrient flux. Therefore, the primary productivity is reduced as spring progresses to summer, and the 0.2 mg/m^3 chlorophyll front moves poleward to between 34°N and 35°N.

Analyzing the OCTS and SeaWiFS data between January 1997 and December 1999, Polovina *et al*. (2001) have found there was considerable interannual variation in the positions of the TZCF, with the largest seasonal shift of 1000 km during 1998, but a much smaller seasonal migration of the TZCF during 1999 (their figure 9). The modeled 0.2 mg/m^3 chlorophyll fronts (Fig. 3) exhibit a seasonal shift about 700–1000 km in the western and central North Pacific. In the eastern part of the basin, the seasonal migration of the TZCF is less pronounced, which is similar to the pattern reported by Polovina *et al*. (2001). Overall, the modeled seasonal migrations of the TZCF, about 700–1000 km in the western and central Pacific, are comparable with the satellite observations. But the modeled TZCF positions tend to be located more in the southern latitudes than the satellite observations during both seasons. This could be due to the general offset between the modeled surface chlorophyll and the satellite observations. In the model, a constant factor for the entire Pacific basin is used to convert the modeled surface phytoplankton biomass (mmol N/m^3) to chlorophyll (mg/m^3). This conversion factor could vary spatially as well as seasonally, but a lack of information prevents us from assigning this conversion factor as a variable for the present ecosystem model. It should be pointed out that the modeled TZCF represents long term climatological mean conditions, whereas the satellite derived TZCF positions (Polovina *et al*., 2001) are only for the period of 1997–99. There have been some indications that a flip from warm to cool PDO phases may have taken place in 1998 (Mantua and Hare, 2002), which could result in shifting overall positions of the TZCF after 1998.

3.2 Modeled interdecadal variability of the mixed layer depth and Ekman pumping

The variability of the TZCF on the interdecadal timescale can likely be viewed as the manifestation of biological response of both subtropical and subarctic gyres to climate variability. Using a coupled physical-biological model forced with the observed surface wind stress and heat flux, the movement of the TZCF in response to the interdecadal forcing has been resolved, but the modeled physical changes are described first.

The mixed layer depth (MLD) during winter regulates supply of nutrients into the euphotic zone, and consequently a potential increase in the spring phytoplankton transition in the western and central subarctic regions. The MLD is controlled mainly by the strength and spatial pattern of the surface wind stress, and changes in the wind stress are therefore reflected in the modeled MLD. In the model, the MLD is defined as the depth at which potential density (σ_t) is 0.125 kg/m^3 higher than its surface value at each grid point. The winter time (January–March) MLD is averaged over two periods, 1979–90 and 1964–75, in order to detect the modeled interdecadal changes, Figs. 4(a) and (b). The model reproduces winter MLD patterns similar to those observed (Monterey and Levitus, 1997) and to other circulation modeling results (Kawamiya *et al*., 2000a, their figure 5a). In general, the maximum MLD is located in the Kuroshio-Oyashio extension region in the northwestern Pacific, with values exceeding 200 m. In the central and northeastern Pacific, the winter MLD ranges between 50 and 100 m. Despite the coarse resolution of the circulation model, $1° \times 2°$ in the mid and high latitude, the simulated MLD seems reasonable. One of the model improvements is incorporation of the nonlocal KPP mixing scheme, which does a better job of capturing the small-scale physics within the upper mixed layer and interior internal waves (Large *et al*., 1994; Li *et al*., 2001). Because of the improvements to the mixed layer dynamics, the coarse resolution circulation model also seems to be able to capture the upper thermal structure changes on interannual-to-interdecadal time scale. For the Kuroshio Current Extension region (34°–42°N, 140°E–180°), Li *et al*. (2001) compared the modeled monthly temperature anomalies with the observations by Deser *et al*. (1996), and found similar trend and magnitude of changes of temperature in the top 400 m from 1970 to 1991 (their figure 14).

A major climatic regime shift occurred in the mid-1970s. The Aleutian Low pressure system intensified and subtropical westerly winds strengthened (Trenberth and

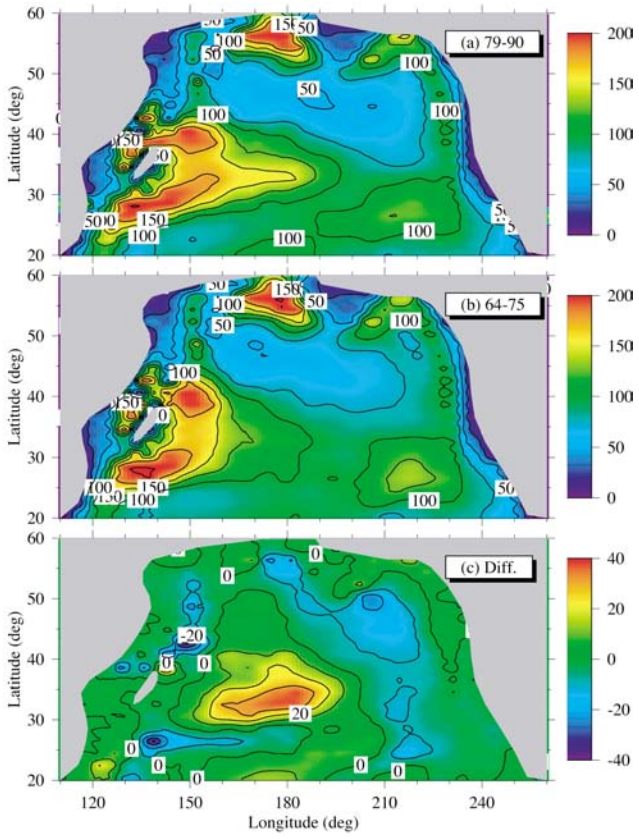

Fig. 4. The modeled winter (January–February–March) mixed layer depth (meters) during the period of 1970–90 (a) and 1964–75 (b). The difference (a–b) between 1979–90 and 1964–75 (c). In (c), positive values mean deeper MLD, for example, 20 equals 20 meters deeper in the MLD.

Hurrell, 1994), which cause the winter and spring MLD to increase by 30–80% in the subtropical gyre and the transition zone (Polovina *et al*., 1995). The modeled winter MLD difference between 1979–90 and 1964–75 shows the greatest increase, located between 30°N and 40°N in the central Pacific (150°E to 180°), with a value of 40–60% higher (deeper mixed layer) during 1979–90 relative to 1964–75 values, Fig. 4(c). In the subarctic gyre (north of 40°N) in both the northeastern Pacific (Ocean Station Papa) and the Oyashio region (northwestern Pacific), the modeled MLD decreases by about 20% during the period 1979–90 relative to 1964–75 levels. Several studies based upon the historical hydrographic data have detected a gradual decrease of the winter MLD during the past several decades both in the eastern (Freeland *et al*., 1997) and western (Ding and Saino, 1999) subarctic North Pacific. The modeled winter MLD changes in the northeastern (Ocean Station Papa) and northwestern (Oyashio region) Pacific agree with the observed declining trend of the winter MLD.

The modeled winter MLD difference closely resembles the spatial patterns and the magnitude of change of findings based upon the NODC temperature profile data published by Polovina *et al*. (1995, their figure 3). The model is designed to capture the basin-scale and long term variability, and the coastal dynamics might not be well resolved. For example, in the Gulf of Alaska, where the modeled MLD difference between 1979–90 and 1964–75 is relatively small, the NODC data indicates a MLD about 20–30% shallower in the winter and spring during the period 1977–88 (Polovina *et al*., 1995). Unlike the treatment of the surface heat flux calculation, the present model is always forced with the monthly averaged climatological salinity values, hence there is no interdecadal signal in the modeled surface salinity field. Haigh *et al*. (2001) analyzed the NODC salinity data for two different periods, 1952–75 and 1977–88, and found that overall the surface water in the subarctic region and the Gulf of Alaska was fresher after 1976–77, which could contribute even more to the shallowing of the MLD in these regions. The role of surface salinity changes on an interdecadal time scale should be considered in future circulation model simulations.

In spite of the coarse resolution of the present circulation model and lack of surface salinity variability on the interdecadal timescale, overall the model produces winter MLD changes before and after the 1976–77 climatic shift that are very similar to the NODC observational data (Polovina *et al*., 1995; Deser *et al*., 1996) as well as other circulation model results (Miller and Schneider, 2000; Xie *et al*., 2000).

Although the circulation model with the KPP scheme has made a significant improvement in simulating the interdecadal variability in the mixed layer dynamics as well as the upper ocean thermal structures, there is sill room for improvement. The overall circulation model can be improved by increasing horizontal resolution in order to resolve some local dynamics, such as the Kuroshio-Oyashio transition zone. The present coarse resolution circulation model is insufficient to adequately reproduce the Kuroshio detachment (Kobayashi, 1999), and this issue could be important for a description of the formation of water masses spreading into the entire subtropical gyre. Thus, resolving the Kuroshio-Oyashio transition zone dynamics is relevant not only to the mixed layer dynamics in the local region alone, but also to other regions as well. Another improvement for future circulation modeling is the sensitivity of the KPP scheme to salinity and freshwater flux and its potential impact on simulating the interdecadal thermal variability, which requires a better evaporation and precipitation fields at ocean surface.

The wind stress curl (the spatial pattern in the surface wind stress) determines the Ekman pumping veloc-

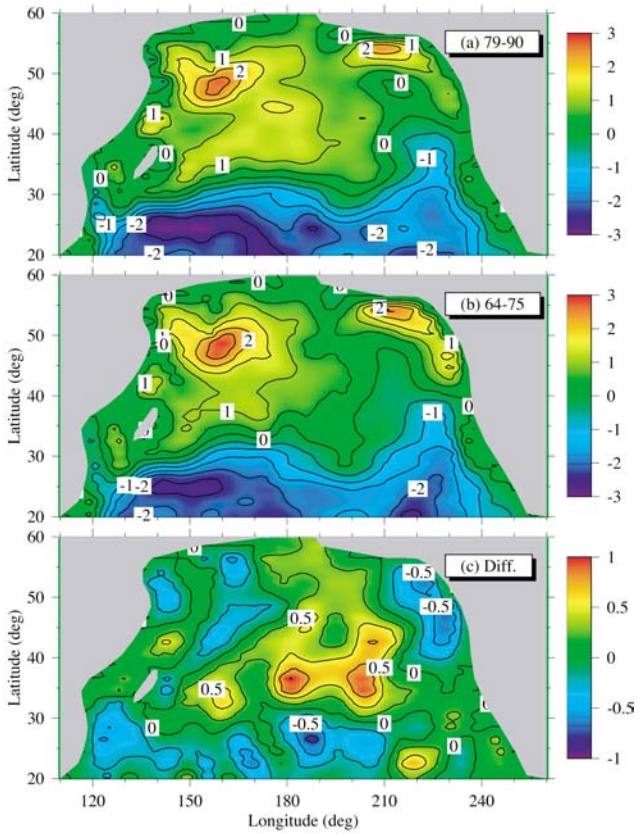

Fig. 5. The winter (January–February–March) Ekman pumping velocity (1×10^{-6} m/sec) during the period of 1979–90 (a) and 1964–75 (b), the positive is upward motion. The difference (a–b) between 1979–90 and 1964–75 (c). In (c), positive values mean stronger Ekman pumping velocity.

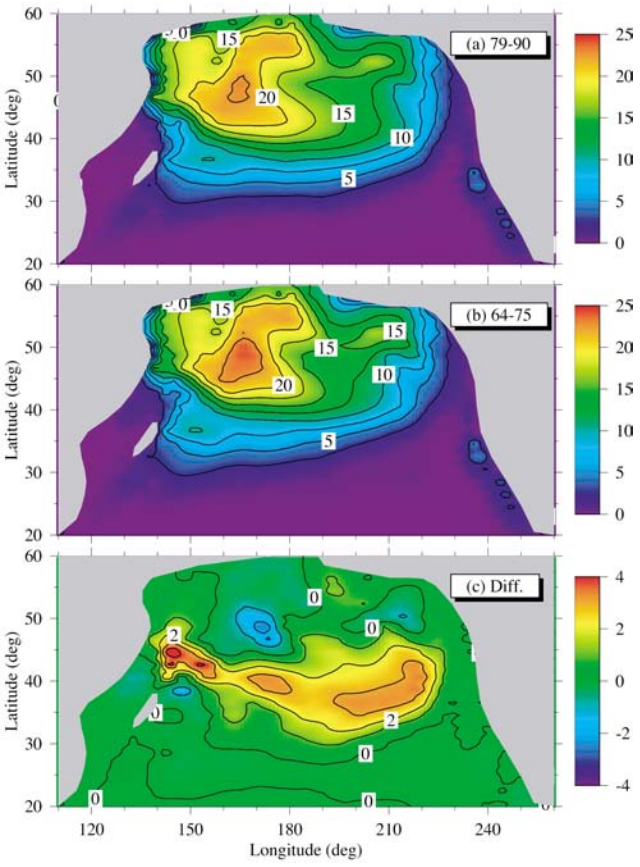

Fig. 6. The modeled winter (January–February–March) surface nitrate concentration (mmol/m^3) during the period of 1979–90 (a) and 1964–75 (b). The difference (a–b) between 1979–90 and 1964–75 (c). In (c), positive values mean increase in the surface nitrate concentration.

ity which directly forces the thermocline. The Ekman pumping velocity (upward positive) is defined as:

$$W_e = \text{curl}(\tau/f)/\rho = [\text{curl}(\tau) + \tau_x \beta/f]/(f\rho). \qquad (1)$$

Here τ is the wind stress, τ_x its zonal component, ρ water density, and β is the latitudinal derivative of the Coriolis parameter. Variability in the Ekman pumping velocity, a reflection of both the wind stress curl and the zonal wind stress, not only impacts the thermocline variation but also influences the depth of the nutricline and thus, furthermore, the phytoplankton productivity. Examining the decadal variability of the Ekman pumping velocity elucidates the winter nutrient concentration changes in the upper ocean which determines intensity of the spring phytoplankton bloom. The annual mean Ekman velocity follows the winter time (January–March) Ekman velocity very closely, but its intensity is reduced compared to the winter time value. Therefore, the winter time Ekman pumping velocity is presented for discussion.

The winter (January–March) Ekman pumping velocity is averaged over two periods, 1979–90 and 1964–75, Figs. 5(a) and (b). The positive Ekman pumping dominates the subarctic gyre with two maxima centered in both western and eastern regions. In the transition zone, between 30°N and 45°N, the winter Ekman pumping velocity is positive overall except in a smaller region in the eastern part of the basin away from the coast. The upward Ekman pumping in the transition zone brings nutrients to the euphotic zone that sustains phytoplankton production in the transition zone and pushes the surface chlorophyll front equatorward during the winter (Fig. 3). In the subtropical gyres, south of 30°N, the Ekman pumping velocity is negative (downward). The overall downward motion in the thermocline depth causes a lack of nutrient supply and limits phytoplankton production in the subtropical gyres (Fig. 2). There is a zonal difference in the Ekman pumping velocity in the subtropical gyres with more intensified downward motion in the west and

less in the east. The winter Ekman pumping velocity field in the subtropical gyres is consistent with the calculation based upon the historical hydrographical data by Suga *et al*. (2000, their figure 16).

The difference in the winter Ekman pumping velocity between 1979–90 and 1964–75 shows the largest increase located between 30°N and 45°N in the central and eastern Pacific (180° to 150°W), Fig. 5(c). The maximum increase of the winter Ekman pumping velocity centered along 35°N is more than doubled during 1979–90 relative to the 1964–75 values. Compared to the largest difference of the modeled winter MLD (150°E to 180°, Fig. 4(c)), the maximum increase of the winter Ekman pumping velocity locates further to the east (170°E to 150°W), and both are found in the latitudinal band between 30°N and 45°N, i.e., the transition zone. In the subarctic northeastern region including the Gulf of Alaska, the winter Ekman pumping velocity decreases by about 25% during the period of 1979–90 relative to 1964–75 levels. In the region south of 30°N, the downward Ekman pumping strengthens during the period of 1979–90, which produces the negative anomalies in the most areas of that region (Fig. 5(c)). The spatial pattern of the winter Ekman pumping velocity difference is complex in the North Pacific, and it is caused by the surface wind stress changes during different decades. Analyzing the NCEP reanalysis wind stress from 1958 to 1997, Xie *et al*. (2000) found a similar spatial pattern and its interdecadal variations for the Ekman pumping velocity (their figures 11 and 12). This provides evidence that the COADS wind stress and wind stress curl are not unique or biased in terms of the interdecadal variability.

Both NCEP reanalysis and COADS wind stress result in very similar Ekman pumping velocity and associated interdecadal variations, but causes for the wind stress changes on interdecadal timescale are still unclear. Miller *et al*. (2003) discuss and summarize several mechanisms responsible for interdecadal climate variations over the Pacific Ocean, including the potential influence of the oceanic biological processes that might have a significant feedback to the physical climate system. In this paper, we focus on the direct biological response to the interdecadal physical forcing, the potential feedback from the oceanic ecosystem to the physical processes is not included in this modeling study.

3.3 Modeled interdecadal variability of the nutrient and primary productivity

The positive upward Ekman pumping and deeper MLD during the winter in the western and central subarctic gyres and the transition zone elevate the surface nutrient concentration, which sets up necessary conditions for enhanced phytoplankton productivity in the spring. The winter (January–March) modeled surface nitrate concentration is averaged over two periods, 1979–90 and 1964–75, Figs. 6(a) and (b). The highest winter surface nitrate concentration is in the northwestern Pacific between 45°N–55°N and 150°E–180°, with the surface values exceeding 20 mmol/m^3. In the northeastern Pacific, for example near the Ocean Station Papa (OSP) (50°N and 145°W), the modeled winter nitrate concentration is about 15 mmol/m^3, which agrees with the OSP winter nitrate value of 15.8 mmol/m^3 (Harrison, 2002, his table 1). In addition to the strong north-south gradient, the east-west contrast of the modeled surface nitrate in the subarctic gyre (north of 40°N) is also pronounced. Overall, the model produces the winter surface nitrate distribution and concentration comparable to the NODC WOA98 (Conkright *et al*., 1998), and especially agrees with the surface nitrate observations collected through the Canada-Japan ship-of-opportunity program between January 1996 and January 2001 (Wong *et al*., 2002, their figure 3d). The modeled surface nitrate concentration also compares well with other physical-biological modeling studies of the North Pacific (Kawamiya *et al*., 2000a, their figure 7; Haigh *et al*., 2001, their figure 2).

The modest interdecadal physical variability affects the nutrient supply to the euphotic zone, which in turn affects phytoplankton productivity and, eventually, higher trophic levels (Venrick *et al*., 1987; McGowan *et al*., 1998). The modeled winter surface nitrate difference between 1979–90 and 1964–75 shows an increase in the latitudinal band of 30°N and 45°N from the west to the east (135°E–135°W), with two maxima (about 4 mmol/m^3) located in the north of Japan (45°N and 140°E) and central northeastern Pacific (40°N and 150°W). The modeled nitrate concentration is about 10 to 50% higher in general during the period of 1979–90 relative to 1964–75 values, depending upon locations. The increase is found mainly along the 10 mmol/m^3 isopleth of nitrate concentration during the 1964–75 period, which indicates the 10 mmol/m^3 isopleth of the modeled nitrate moves equatorward during 1979–90. From the perspective of nitrate increase after 1976–77, the subarctic gyre expanded which resulted in an increase of surface nitrate concentration in the transitional zone (30°N to 45°N) during 1979–90. The winter surface nitrate concentration difference (Fig. 6(c)) is caused by a combination of the winter MLD difference (Fig. 4(c)) and winter Ekman pumping velocity difference (Fig. 5(c)), and seems to follow the latter more closely.

The spatial distribution of the modeled surface nitrate concentration difference is consistent with several direct and indirect observations. For example, in the central North Pacific, Venrick *et al*. (1987) found that the average euphotic zone (0–200 m) chlorophyll concentration in the oligotrophic region during summer (May–October) had nearly doubled from 1968 to 1985. Their data

collected from the Climax region (26.5–31.0°N and 150.5–158.0°W) also indicated a decrease in sea surface temperature, which suggests an increase in surface nutrients. The area of the largest increase in the modeled winter surface nitrate is between 30°N and 45°N, and it varies longitudinally. The very southern edge of the modeled surface nitrate changes overlaps with the northern edge of the Climax region (31°N). Since the modeled surface nitrate focuses on the winter season (January–March), and the insufficiently sampled Climax data was mainly for the summer season (May–October), it is difficult to make a direct and detailed comparison between the modeled results and the Climax observations. Combining the data collected from the ongoing Hawaii Ocean Time series (HOT) program and the Climax data for the North Pacific Subtropical Gyre, Karl *et al*. (2002) have also stated that mean euphotic zone chlorophyll concentration from the period October 1988 to December 1997 is also significantly greater than the averaged pre-1976 Climax program chlorophyll concentration (their figure 9.12). Unfortunately, our model simulation ends at December 1993 due to a lack of processed COADS surface observations after 1993. A direct comparison with the HOT observations could not be done with our current model simulations. It seems that the largest decadal variations occurred in the north of HOT and Climax regions according to the modeled results, but there are no other direct, consistent observational data in these areas to confirm such findings at present.

Analyzing and comparing oxygen utilization (AOU) from four meridional transects along 152°W (or 155°W) between 45°N and Hawaii during the past two decades, Emerson *et al*. (2001) found an increase of AOU by 20–25% and this could result from an increase in biological productivity. Ono *et al*. (2001) analyzed the hydrographic observations (only winter data was selected) from 1968 to 1998 in the Oyashio region (39°N to 43°N, 143°E to 149°E) and found that there was a linear increasing trend in both phosphate and AOU in the subsurface (deeper than 100 m), which agrees with our modeled nitrate difference (not shown for the subsurface difference). Moreover, Ono *et al*. (2001) suggested that the linear increasing trend in subsurface phosphate and AOU may not be caused by the bidecadal oscillation (20 years) but may correspond to the longer-term process such as pentadecadal (50 years, e.g. Minobe, 1999) or anthropogenic effects. On the other hand, Ding and Saino (1999) found that the winter MLD in the same location (the Oyashio region) had decreased since 1968, and our modeled winter MLD shows a similar trend (Fig. 4(c)). Ding and Saino (1999) also found that nutrient concentration in the mixed layer decreased whereas our modeled result shows an increase in the surface nitrate in that region (Fig. 6(c)). The modeled surface nitrate increases due to the positive anomaly of the winter Ekman pumping velocity between 1979–90 and 1964–75 (see Fig. 5(c)). Even though the winter MLD shallowed in the Oyashio region after 1976–77, the enhanced winter Ekman pumping in this region pushes the subsurface nitricline upward which results in the increase in the subsurface nitrate, and potentially surface nitrate, too. More detailed model and data comparisons are needed for the regions where historical hydrographic data exist, especially for any long term changes in the vertical structure.

In the northeastern Pacific, for example the Ocean Station Papa (OSP, 50°N and 145°W), Freeland *et al*. (1997) found that the observed winter nitrate concentration within the upper 100 m had decreased since 1970 with a declining trend of about 16.3 mmol/m^3/century (their figure 7). The modeled winter surface nitrate concentration at the OSP changed about 2 mmol/m^3 between 1979–90 and 1964–75 (Fig. 6(c)), which agrees well with the observed declining rate. The shallowing in the winter MLD at the OSP, due to the combination of warming and freshening at sea surface, caused an overall reduction in nitrate concentration in the upper ocean (Freeland *et al*., 1997). In the model, the winter surface nitrate decreasing trend at the OSP is caused by the combination of the winter MLD decrease (Fig. 4(c)) and a negative anomaly of the winter Ekman pumping (Fig. 5(c)) which reduces the upward Ekman motion after 1976–77. Further examination of the changes in the vertical nutrient profiles at the OSP may yield more information about the interdecadal variability of upward nutrient flux, and thus productivity and biomass changes at the OSP.

The spatial pattern of the modeled winter nitrate difference between 1979–90 and 1964–75 is complex; it is mainly associated with the large scale wind pattern changes both in wind stress intensity and wind stress curl. The change in the surface nitrate concentration certainly has an impact on phytoplankton productivity and surface chlorophyll distribution. Since the interdecadal variation of the TZCF is one of the focuses of this paper, we concentrate our analysis on the modeled productivity changes in the NPTZ.

In the central North Pacific, 30°N–40°N and 180°–140°W, the modeled vertically integrated (0–100 m) primary production anomaly was obtained by removing the seasonal cycle and then a 7-year running mean was applied to the anomaly field in order to remove the interannual variability, Fig. 7(a). Overall, the modeled primary production anomaly tracks the Pacific Decadal Oscillation (PDO) index very closely, with lower productivity during the negative PDO phase before 1976–77 and higher production values thereafter. In the region defined above, the area averaged mean seasonal cycle of the integrated (0–100 m) primary production ranges from 10.1 mmol C/m^2/day in the winter to 40.5 mmol C/m^2/day in

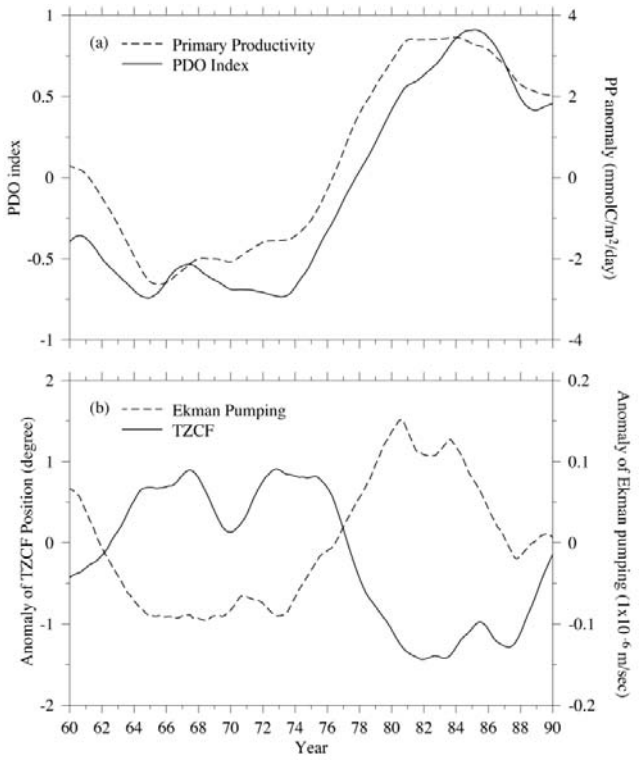

Fig. 7. (a) PDO index and primary production (PP) anomaly in the central North Pacific (30°N–40°N and 180°–140°W). The PDO Index is defined as the leading principal component of North Pacific monthly sea surface temperature variability (poleward of 20°N for the 1900–93 period), see http://tao.atmos.washington.edu/pdo/ for more details (Mantua and Hare, 2002), courtesy of Dr. Nathan Mantua at University of Washington. The monthly averaged PP anomaly was derived by removing the seasonal cycle (it includes all seasons, not just winter time). Both PDO and PP anomaly were smoothed with 7 year and 2 year running mean filters. (b) The anomaly of Ekman pumping velocity in the central North Pacific and TZCF (chlorophyll = 0.2 mg/m^3) anomaly (latitudinal, in degree) averaged between 180°–140°W. Again, both anomalies were derived by removing seasonal cycles and then smoothed with the same running filters as in (a). It includes all the seasons, not just the wintertime. The positive anomaly means the TZCF moves northward, and negative anomaly means the equatorward movement.

the spring, with an annual mean value of 29.8 mmol C/m^2/day. The amplitude of modeled primary production anomaly is 6.3 mmol C/m^2/day with the highest value of 3.6 mmol C/m^2/day during the early 1980s and the lowest value of –2.7 mmol C/m^2/day during the mid-1960s. Before and after the 1976–77 climate shift, the modeled primary productivity increased by about 21% relative to the annual mean values (6.3/29.8 = 0.21).

The modeled primary productivity increase is caused by the enhanced surface nitrate in the central North Pacific (Fig. 6(c)). The sharp increase in the modeled primary productivity occurs around 1976–77 when the PDO index switches from negative to positive, which causes an increase of the winter MLD and strengthened Ekman pumping. This indicates that the lower trophic primary producers in the marine ecosystem respond to the physical climate changes quickly, and the productivity tends to stay in one mode for a couple of decades or so before switching to the opposite phase. Such sudden switches in primary productivity seem to play an important role in determining which small pelagic fish dominate, as in the anchovy and sardine alternation at similar periods of around 20 years (Chavez *et al*., 2003).

Enhanced primary productivity after the 1976–77 climatic shift contributes higher phytoplankton biomass and therefore elevates chlorophyll level in the central North Pacific. An increase in the modeled chlorophyll concentration expands the high chlorophyll area in the NPTZ and pushes the TZCF equatorward. In order to detect the TZCF position changes, the anomaly field of the 0.2 mg/m^3 surface chlorophyll monthly position (which includes all seasons, not just wintertime) was obtained by removing its seasonal cycle and applying a long-term running mean filter (Fig. 7(b)). As a reference for the interdecadal changes, the anomaly field of the Ekman pumping velocity averaged over the region (30°N–40°N and 180°–140°W) has also been plotted in Fig. 7(b). Prior to the 1976–77 climate shift, the 0.2 mg/m^3 surface chlorophyll front is located 1° northward (positive anomaly) from the long-term mean positions (0° line). After the 1976–77 shift, the 0.2 mg/m^3 surface chlorophyll front moves southward about 1.5° (negative anomaly) the during 1980s. The amplitude of north-south migration of the 0.2 mg/m^3 surface chlorophyll front is about 2.5° (about 250 km) between 1964–75 and 1979–90. After the 1976–77 climatic shift, the higher chlorophyll area in the NPTZ expanded and the TZCF migrated equatorward from the long term mean position.

The location of the TZCF appears to be related to juvenile albacore tuna migration patterns within the transition zone and this has potential implications for albacore fishery. Polovina *et al*. (2001) found that the 3–5 year-old albacore being caught by the troll fishing fleet are exploiting the TZCF as migration route and as forage habitat during their trans-Pacific migration. Furthermore, they found that both albacore fishing effort and the highest albacore catch-per-unit of effort (CPUE) are concentrated along the TZCF (their figure 5, Polovina *et al*., 2001). The interdecadal movement of the TZCF is important, especially its relationship to the fishery, but this is very difficult to confirm directly with surface chlorophyll measurements. The high quality remote sensing

ocean color data, i.e., SeaWiFS and OCTS, are available only for the past several years (1997 to present). There is a big gap between the CZCS data set (1978–86) and the SeaWiFS, so detecting the interdecadal migration of the TZCF using the remote sensing data is not possible at present. Historical fishery catch data near the TZCF might yield some information on how the TZCF migrated during the past several decades, which may provide a test for the physical-biological model results regarding the interdecadal movement of the TZCF. Such a study is needed in order to improve physical-biological model performance and reliability, as well as to accurately assess climatic and human influences on the marine ecosystem.

4. Conclusions

A three-dimensional physical-biological model has been used to study interdecadal variation of the transition zone chlorophyll front (TZCF) in the central North Pacific Ocean. The physical model is a modified version of Modular Ocean Model (MOM 1.0, Pacanowski *et al*., 1991), configured for the Pacific Ocean by Li *et al*. (2001). The biological model was developed originally for the equatorial Pacific Ocean to study the nitrogen and silicon cycles by Chai *et al*. (2002) and Dugdale *et al*. (2002). The physical-biological model is forced with the monthly mean heat flux and surface wind stress from the Comprehensive Ocean Atmosphere Data Set (COADS) (da Silva *et al*., 1994). The physical-biological model results from the 30-year (1960–1990) retrospective analysis are as follows:

1) The modeled spring surface chlorophyll concentration reproduces the *in situ* chlorophyll observations in the western and central subartic regions, including the position of the TZCF, defined as the isopleth of 0.2 mg/m^3 surface chlorophyll. The modeled TZCF is located between 26°N and 27°N in the central North Pacific during winter and between 34°N and 35°N during the summer, which tends to agree with the satellite observed seasonal migration patterns of the TZCF (Polovina *et al*., 2001).

2) The interdecadal variability of modeled winter MLD shows the largest increase which is located between 30°N and 40°N in the central North Pacific (150°E to 180°), with a value of 40–60% higher (deeper mixed layer) during 1979–90 relative to 1964–75 values. In the subarctic gyre in both northeast (Ocean Station Papa) and northwest Pacific (Oyashio region), the modeled winter MLD decreases by about 20% during the period of 1979–90 relative to 1964–75 levels. Overall, the model produces the winter MLD changes before and after the 1976–77 climatic shift, which are very similar to the historical observational data (Polovina *et al*., 1995; Deser *et al*., 1996).

3) The interdecadal variability of the winter Ekman pumping velocity difference between 1979–90 and 1964–75 shows the largest increase which is located between 30°N and 45°N in the central and eastern North Pacific (180° to 150°W). In the subarctic northeast Pacific region including the Gulf of Alaska, the winter Ekman pumping velocity decreases during the period 1979–90, but its value increases in the northwest Pacific (Oyashio region) after the 1976–77 climatic shift. The Ekman pumping velocity difference before and after 1976–77 derived from the COADS surface wind stress agree with the results based upon the NCEP reanalysis by Xie *et al*. (2000).

4) The physical-biological model produces winter surface nitrate concentration comparable to the observed values (Conkright *et al*., 1998; Wong *et al*., 2002). The modeled winter surface nitrate difference between 1979–90 and 1964–75 shows an increase in the latitudinal band between 30°N and 45°N from the west to the east (135°E–135°W), the modeled nitrate concentration is about 10 to 50% higher in 1979–90 relative to 1964–75. The increase of the winter surface nitrate concentration during 1979–90 is caused by a combination of the winter MLD increase and the winter Ekman pumping enhancement after the 1976–77 climatic shift.

5) The modeled nitrate concentration increases after the 1976–77 climate shift results in increasing primary productivity in the central North Pacific (30°N–40°N and 180°–140°W). Enhanced primary productivity after the 1976–77 climatic shift contributes higher phytoplankton biomass and therefore elevates chlorophyll level in the central North Pacific. Increased chlorophyll expands the high chlorophyll area and pushes the TZCF equatorward. The amplitude of north-south migration of the 0.2 mg/m^3 surface chlorophyll front is about 250 km between 1964–75 and 1979–90.

Acknowledgements

This research was supported by NASA and NSF Grants to F. Chai. Two anonymous reviewers provided comments that greatly improved the final version of the manuscript. F. Chai thanks Drs. T. Saino and K. Suzuki for the discussions during his sabbatical at Nagoya University. This publication is U.S. JGOFS contribution No. 863.

References

Barber, R. T. and F. P. Chavez (1991): Regulations of primary productivity rate in the equatorial Pacific. *Limnol. Oceanogr*., **36**(8), 1803–1815.

Barber, R. T., S. T. Lindley, M. Sanderson, F. Chai, J. Newton, C. C. Trees, D. G. Foley and F. Chavez (1996): Primary production in the equatorial Pacific during 1992. *Deep-Sea Res. II*, **42**, No. 4–6, 933–969.

Bidigare, R. R. and M. E. Ondrusek (1996): Spatial and temporal variability of phytoplankton pigment distributions in the central equatorial Pacific Ocean. *Deep-Sea Res. II*, **43**, 809–833.

Chai, F. (1995): Origin and maintenance of high nutrient condition in the Equatorial Pacific, a biological-physical model study. Ph.D. Dissertation, Duke University, 170 pp.

Chai, F., S. T. Lindley and R. T. Barber (1996): Origin and maintenance of a high NO_3 condition in the equatorial pacific. *Deep-Sea Res. II*, **43**, 1031–1064.

Chai, F., S. T. Lindley, J. R. Toggweiler and R. T. Barber (1999): Testing the importance of iron and grazing in the maintenance of the high nitrate condition in the Equatorial Pacific Ocean, a physical-biological model study. In *The Changing Ocean Carbon Cycle*, ed. by R. B. Hanson, H. W. Ducklow and J. G. Field, International Geosphere-Biosphere Programme (IGBP) Book Series 5, p. 156–186, Cambridge University Press.

Chai, F., R. C. Dugdale, T.-H. Peng, F. P. Wilkerson and R. T. Barber (2002): One dimensional ecosystem model of the Equatorial Pacific upwelling system, Part I: Model development and silicon and nitrogen cycle. *Deep-Sea Res. II*, **49**, No. 13–14, 2713–2745.

Chavez, F. P., J. Ryan, S. Liuch-Cota and M. Niquen (2003): From Anchovies to Sardines and back—multidecadal change in the Pacific Ocean. *Science*, **299**, 217–221.

Coale, K. H. *et al*. (1996): A massive phytoplankton bloom induced by an ecosystem-scale iron fertilization experiment in the equatorial Pacific Ocean. *Nature*, **838**, 495–501.

Conkright, M., T. O'Brien, M., S. Levitus, T. P. Boyer, J. Antonov and C. Stephens (1998): World Ocean Atlas 1998 Vol. 11: Nutrients and Chlorophyll of the Pacific Ocean. NOAA Atlas NESDIS 37, U.S. Gov. Printing Office, Washington, D.C., 245 pp.

da Silva, A. M., C. C. Young-Molling and S. Levitus (1994): Atlas of Surface Marine Data 1994, Vol. 1: Algorithms and Procedures. NOAA Atlas NESDIS 6, U.S. Gov. Printing Office, Washington, D.C., 83 pp.

Denman, K. L. and M. A. Pena (1999): A coupled 1-D biological/physical model of the northeast subarctic Pacific Ocean with iron limitation. *Deep-Sea Res. II*, **46**, 2877–2908.

Deser, C., M. A. Alexander and M. S. Timlin (1996): Upper-Ocean Thermal Variations in the North Pacific during 1970–1991. *J. Climate*, **9**, No. 8, 1840–1855.

Ding, L.-J. and T. Saino (1999): Seasonal and long-term interannual variations of biological environments in Oyashio surface waters off Tohoku prefecture, Japan. In *Proceedings of 1999 Spring Meeting of the Oceanographic Society of Japan*, Oceanographic Society of Japan, Tokyo, Japan, 156 pp.

Dugdale, R. C., R. T. Barber, F. Chai, T. H. Peng and F. P. Wilkerson (2002): One dimensional ecosystem model of the Equatorial Pacific upwelling system, Part II: Sensitivity analysis and comparison with JGOFS EqPac data. *Deep-Sea Res. II*, **49**, No. 13–14, 2746–2762.

Emerson, S., S. Meching and J. Abell (2001): The biological pump in the subtropical North Pacific Ocean: nutrient sources, Redfield ratios, and recent changes. *Glob. Biogeochem. Cyc.*, **15**, 535–554.

Favorite, F., A. J. Dodimead and K. Nasu (1976): Review of the oceanography of the North Pacific, 1960–1971. *Bull. Int. North Pacific Fish. Commun.*, **33**, 1–187.

Francis, R. C. and S. R. Hare (1994): Decadal-scale regime shifts in the large marine ecosystems of the North-east Pacific: a case for historical science. *Fish. Oceanogr.*, **3**, 279–291.

Freeland, H. J., K. Denman, S. S. Wong, F. Whitney and R. Jacques (1997): Evidences of change in the winter mixed layer in the Northeast Pacific Ocean. *Deep-Sea Res.*, **44**, 2117–2129.

Frost, B. W. and N. C. Franzen (1992): Grazing and iron limitation in the phytoplankton stock and nutrient concentration: a chemostat analogue of the Pacific equatorial upwelling zone. *Mar. Ecol. Prog. Ser.*, **83**, 291–303.

Frost, B. W. and M. J. Kishi (1999): Ecosystem dynamics in the eastern and western gyres of the Subarctic Pacific—a review of lower trophic level modeling. *Prog. Oceanogr.*, **43**, 317–333.

Gent, P. and J. C. McWilliam (1990): Isopycnal mixing in ocean circulation models. *J. Phys. Oceanogr.*, **20**, 150–155.

Gent, P. R., F. O. Bryan, G. Danabasoglu, S. C. Doney, W. R. Holland, W. G. Large and J. C. McWilliams (1998): The NCAR climate system model global ocean component. *J. Climate*, **11**, 1287–1306.

Graham, N. E. (1994): Decadal-scale climate variability in the tropical and North Pacific during the 1970s and 1980s: Observations and model results. *Clim. Dyn.*, **10**, 135–162.

Haigh, S. P., K. L. Denman and W. W. Hsieh (2001): Simulation of the planktonic ecosystem response to pre- and post-1976 forcing in an isopycnic model of the North Pacific. *Can. J. Fish. Aquat. Sci.*, **58**, 703–722.

Harrison, P. J. (2002): Station Papa time series: Insights into ecosystem dynamics. *J. Oceanogr.*, **58**, 259–264.

Holland, W. R., J. J. C. Chow and F. O. Bryan (1998): Application of a third-order upwind scheme in the NCAR ocean model. *J. Climate*, **11**, 1487–1493.

Jiang, M.-S., F. Chai, R. C. Dugdale, F. Wilkerson, T.-H. Peng and R. T. Barber (2003): A nitrate and silicate budget in the equatorial Pacific Ocean: A coupled biological-physical model study. *Deep-Sea Res. II*. (in press).

Karl, D. M., R. R. Bidigae and R. B. Letelier (2001): Long-term changes in plankton community structure and productivity in the North Pacific subtropical gyre: The domain shift hypothesis. *Deep-Sea Res. II*, **48**, 1449–1470.

Karl, D. M., R. R. Bidigae and R. B. Letelier (2002): Sustained and aperiodic variability in organic matter production and phototrophic microbial community structure in the North Pacific subtropical gyre. p. 222–264. In *Phytoplankton Productivity: Carbon Assimilation in Marine and Freshwater Ecosystems*, ed. by P. J. Le B. Williams, D. N. Thomas and C. S. Reynolds, Blackwell Science.

Kawamiya, M., M. J. Kishi and S. Suginohara (2000a): An ecosystem-physical combined model for the North Pacific. Part 1: Model description and the characteristics of the spatial distributions of biological variables. *J. Mar. Syst.*, **25**, 129–157.

Kawamiya, M., M. J. Kishi and S. Suginohara (2000b): An ecosystem-physical combined model for the North Pacific. Part

II: Mechanisms of the season variation of chlorophyll. *J. Mar. Syst*., **25**, 159–178.

Kobayashi, T. (1999): Study of the formation of North Pacific Intermediate Water by a general circulation model and the particle-tracking method 1. A pitfall of general circulation model studies. *J. Geophys. Res*., **104**, No. 3, 5423–5439.

Landry, M. R., R. T. Barber, R. R. Bidigare, F. Chai, K. H. Coale, H. G. Dam, M. R. Lewis, S. T. Lindley, J. J. McCarthy, M. R. Roman, D. K. Stoecker, P. G. Verity and J. R. White (1997): Iron and grazing constraints on primary production in the central equatorial Pacific: An EQPAC synthesis. *Limnol. Oceanogr*., **42**, No. 3, 405–418.

Large, W. G., J. C. McWilliams and S. C. Doney (1994): Oceanic vertical mixing: a review and a model with a nonlocal boundary layer parameterization. *Rev. Geophys*., **32**, 363–403.

Levitus, S. and T. Boyer (1994): World Ocean Atlas 1994, Vol. 4: Temperature. NOAA Atlas NESDIS 4, U.S. Gov. Printing Office, Washington, D.C., 117 pp.

Levitus, S., M. E. Conkright, J. L. Reid, R. Najjar and R. G. Mantyla (1993): A distribution of nitrate, phosphate and silicate in the world oceans. *Prog. Oceanogr*., **31**, No. 3, 245–273.

Levitus, S., R. Burgett and T. Boyer (1994): World Ocean Atlas 1994, Vol. 3: Salinity. NOAA Atlas NESDIS 3, U.S. Gov. Printing Office, Washington, D.C., 99 pp.

Li, X., Y. Chao, J. C. McWilliams and L.-L. Fu (2001): A comparison between two vertical mixing schemes in a Pacific OGCM. *J. Climate*, **14**, No. 7, 1377–1398.

Limsakul, A., T. Saino, T. Midorikawa and J. I. Goes (2001): Temporal variations in lower trophic level biological environments in the northwestern North Pacific Subtropical Gyre from 1950 to 1997. *Prog. Oceanogr*., **49**, 129–149.

Longhurst, A. (1998): *Ecological Geography of the Sea*. Academic Press, San Diego, 391 pp.

Lynn, R. J. (1986): The subarctic and northern subtropical fronts in the eastern North Pacific Ocean in spring. *J. Phys. Oceanogr*., **16**, 209–222.

Maldonado, M. T., P. W. Boyd, P. J. Harrison and N. P. Price (1999): Co-limitation of phytoplankton growth by light and Fe during winter in the subarctic Pacific Ocean. *Deep-Sea Res. II*, **46**, 2475–2485.

Mantua, N. J. and S. R. Hare (2002): The Pacific decadal oscillation. *J. Oceanogr*., **58**, 35–44.

Mantua, N. J., S. R. Hare, Y. Zhang, J. M. Wallace and R. C. Francis (1997): A Pacific interdecadal climate oscillation with impacts on salmon production. *Bull. Am. Meteor. Soc*., **78**, 1069–1079.

Martin, J. H. and S. F. Fitzwater (1988): Iron deficiency limits phytoplankton growth in the north-east Pacific subarctic. *Nature*, **331**, 341–343.

Martin, J. H., G. A. Knauer, D. M. Karl and W. W. Broenkow (1987): VERTEX: carbon cycling in the northeast Pacific. *Deep-Sea Res*., **34**(2), 267–285.

McGowan, J. A., D. R. Cayan and L. M. Dorman (1998): Climate-ocean variability and ecosystem response in the northeast Pacific. *Science*, **281**, 210–217.

Miller, A. J. and N. Schneider (2000): Interdecadal climate regime dynamics in the North Pacific Ocean: Theories, observations and ecosystem impacts. *Prog. Oceanogr*., **47**, 355–379.

Miller, A. J., D. R. Cayan, T. P. Barnett, N. E. Graham and J. M. Oberhuber (1994): The 1976–77 climate shift of the Pacific Ocean. *Oceanography*, **7**, 21–26.

Miller, A. J., M. A. Alexander, G. J. Boer, F. Chai, K. Denman, D. J. Erickson, R. Frouin, A. J. Gabric, E. A. Laws, M. R. Lewis, Z. Liu, R. Murtugudde, S. Nakamoto, D. J. Neilson, J. R. Norris, J. C. Ohlmann, R. Perry, N. Schnerider, K. Shell and A. Timmermann (2003): Potential feedbacks between Pacific Ocean ecosystems and interdecadal climate variations. *Bulletin of the American Meteorological Society (BAMS)*, May 2003, 617–633.

Minobe, S. (1999): Resonance in bidecadal and pentadecadal climate oscillations over the North Pacific: Role in climatic regime shifts. *Geophys. Res. Lett*., **26**, 855–858.

Monterey, G. I. and S. Levitus (1997): Seasonal variability of mixed layer depth for the world ocean. NOAA NESDIS Atlas 14, U.S. Gov. Printing Office, Washington, D.C., 5 pp. 87 figs.

Ono, T., T. Midorikawa, Y. W. Watanabe, K. Tadokoro and T. Saino (2001): Temporal increases of phosphate and apparent oxygen utilization in the subsurface waters of western subarctic Pacific from 1968 to 1998. *Geophys. Res. Lett*., **28**, 3285–3288.

Pacanowski, R., K. Dixon and A. Rosati (1991): The GFDL modular ocean model users guide, version 1.0. Tech. Rep. 2, Ocean Group, Geophys. Fluid Dyn. Lab., Princeton.

Polovina, J. J., G. T. Mitchum, N. E. Graham, M. P. Craig, E. E. DeMartini and E. N. Flint (1994): Physical and biological consequences of a climatic event in the Central North Pacific. *Fish. Oceanogr*., **3**, 15–21.

Polovina, J. J., G. T. Mitchum and G. T. Evans (1995): Decadal and basin-scale variation in mixed layer depth and the impact on biological production in the Central and North Pacific, 1960–88. *Deep-Sea Res*., **42**, 1701–1716.

Polovina, J. J., D. R. Kobayashi, D. M. Parker, M. P. Seki and G. H. Balazs (2000): Turtles on the edge: movement of loggerhead turtles (*Caretta caretta*) along oceanic fronts spanning longline fishing grounds in the central North Pacific, 1997–1998. *Fish. Oceanogr*., **9**, 1–13.

Polovina, J. J., E. Howell, D. R. Kobayashi and M. P. Seki (2001): The transition zone chlorophyll front, a dynamic global feature defining migration and forage habitat for marine resources. *Prog. Oceanogr*., **49**, 469–483.

Ragueneau, O., P. Treguer, A. Leynaert, R. F. Anderson, M. A. Brzeinski, D. J. Demaster, R. C. Dugdale *et al*. (2000): *Global and Planetary Change*, **26**, 317–365.

Roden, G. I. (1991): Subarctic-subtropical transition zone of the North Pacific: large-scale aspects and mesoscale structure. p. 1–38. In *Biology, Oceanography and Fisheries of the North Pacific Transition Zone and Subarctic Frontal Zone*, ed. by J. A. Wetherall, NOAA Technical Report. NMFS 105.

Suga, T., A. Kato and K. Hanawa (2000): North Pacific tropical water: its climatology and temporal changes associated with the climate regime shift in the 1970s. *J. Oceanogr*., **47**, 223–256.

Sugimoto, T. and K. Tadokoro (1997): Interannual-interdecadal

variations in zooplankton biomass, chlorophyll concentration and physical environment in the subarctic Pacific and Bering Sea. *Fish. Oceanogr*., **6**, 74–93.

Trenberth, K. E. and J. W. Hurrell (1994): Decadal atmosphere-ocean variations in the Pacific. *Clim. Dyn*., **9**, 303–319.

Venrick, E. L., J. A. McGowan, D. R. Cayan and T. L. Hayward (1987): Climate and chlorophyll a: long-term trends in the central north Pacific Ocean. *Science*, **238**, 70–72.

Wefer, G. (1989): Particle flux in the ocean: effects of episodic production. p. 85–98. In *Productivity of the Ocean; Present and Past*, ed. by W. H. Berger, V. S. Smetacek and G. Wefer, Dahlem Workshop Reports, 44.

Wong, C. S, N. A. Waser, Y. Nojiri, W. K. Johnson, F. A. Whitney, J. S. Page and J. Zeng (2002): Seasonal and interannual variability in the distribution of surface nutrients and dissolved inorganic carbon in the Northern North Pacific: influence of El Niño. *J. Oceanogr*., **58**, 227–243.

Xie, S.-P., T. Kunitani, A. Kubokawa and S. Hosoda (2000): Interdecadal thermocline variability in the North Pacific for 1958–97: A GCM simulation. *J. Phys. Oceanogr*., **30**, No. 11, 2798–2813.